A spherical higher-order finite-difference time-domain algorithm with perfectly matched layer*

Liu Ya-Wen(刘亚文)†, Chen Yi-Wang(陈亦望), Zhang Pin(张 品), and Liu Zong-Xin(刘宗信)

National Key Laboratory on Electromagnetic Environment and Electro-optical Engineering, PLA University of Science and Technology, Nanjing 210007, *China*

(Received 2 April 2014; revised manuscript received 7 May 2014; published online 10 October 2014)

A higher-order finite-difference time-domain (HO-FDTD) in the spherical coordinate is presented in this paper. The stability and dispersion properties of the proposed scheme are investigated and an air-filled spherical resonator is modeled in order to demonstrate the advantage of this scheme over the finite-difference time-domain (FDTD) and the multiresolution time-domain (MRTD) schemes with respect to memory requirements and CPU time. Moreover, the Berenger's perfectly matched layer (PML) is derived for the spherical HO-FDTD grids, and the numerical results validate the efficiency of the PML.

Keywords: higher-order finite-difference time-domain, spherical coordinates, stability, numerical dispersion, perfectly matched layer

PACS: 41.20.Jb, 42.25.Bs, 42.25.Gy **DOI:** 10.1088/1674-1056/23/12/124102

1. Introduction

The higher-order finite-difference time-domain (HO-FDTD) technique[1–13] has been widely used for analyzing the electromagnetic problems such as solving guided wave systems, designing various electrical and electronic devices that involve electromagnetic waves, and characterizing kinds of electromagnetic wave phenomena. Compared with the long established finite difference time-domain (FDTD) algorithm,[14] the HO-FDTD method can greatly reduce the numerical dispersion, which indicates that the HO-FDTD approach is able to use much less memory and CPU time than the FDTD scheme in the electromagnetic computation. Manry *et al.*[1] investigated the use of a second-order in time, sixth-order in space FDTD (2, 6) algorithm. Roberts and Joubert[3] described the implementation and verification of the perfectly matched layer (PML) absorbing boundary condition for the HO-FDTD (2, 4) technique. Lan *et al.*[5] discussed a higher order (2, 4) scheme for the solution of Maxwell's equations (ME's) in time domain, which is employed in modeling wide-band electromagnetic phenomena on a coarse grid. Shao *et al.*[8] proposed an HO-FDTD (2M, 4) method, in which the time differential is of the fourth order and the spatial differential using the discrete singular convolution is of order 2M. Chen *et al.*[13] developed an HO-FDTD with a cylindrical grid for time-domain ME's, and two absorbing boundary conditions were derived for the cylindrical HO-FDTD grids.

In the present paper we extend the HO-FDTD concept to spherical coordinates, and present an HO-FDTD algorithm for solving ME's in spherical grids. For simplicity and generality, the HO-FDTD (2, 6) approach is employed in this work. The stability and dispersion errors of the HO-FDTD scheme are analyzed and compared with those from the FDTD and MRTD schemes based on compactly supported wavelet-Daubechies' scaling functions with two vanishing moments.[15–17] Moreover, the Berenger's PML is derived for the spherical HO-FDTD scheme, of which the absorbing ability is investigated through validation of convergence, symmetry, and an electric dipole near a conductive sphere.

2. HO-FDTD for spherical grid

In this work, a homogeneous medium is considered. Maxwell's vector equations are given by

$$\nabla \times \boldsymbol{E} = -\mu \frac{\partial \boldsymbol{H}}{\partial t} - \sigma_m \boldsymbol{H}, \quad \nabla \times \boldsymbol{H} = \varepsilon \frac{\partial \boldsymbol{E}}{\partial t} + \sigma \boldsymbol{E}. \tag{1}$$

Discretizing Eq. (1) in spherical coordinates as

$$\varepsilon \frac{\partial E_r}{\partial t} + \sigma E_r = \frac{1}{r \sin\theta} \left[\frac{\partial \left(\sin\theta H_\varphi \right)}{\partial \theta} - \frac{\partial H_\theta}{\partial \varphi} \right], \tag{2}$$

$$\varepsilon \frac{\partial E_\theta}{\partial t} + \sigma E_\theta = \frac{1}{r} \left[\frac{1}{\sin\theta} \frac{\partial H_r}{\partial \varphi} - \frac{\partial \left(r H_\varphi \right)}{\partial r} \right], \tag{3}$$

$$\varepsilon \frac{\partial E_\varphi}{\partial t} + \sigma E_\varphi = \frac{1}{r} \left[\frac{\partial \left(r H_\theta \right)}{\partial r} - \frac{\partial H_r}{\partial \theta} \right], \tag{4}$$

$$-\mu \frac{\partial H_r}{\partial t} - \sigma_m H_r = \frac{1}{r \sin\theta} \left[\frac{\partial \left(\sin\theta E_\varphi \right)}{\partial \theta} - \frac{\partial E_\theta}{\partial \varphi} \right], \tag{5}$$

$$-\mu \frac{\partial H_\theta}{\partial t} - \sigma_m H_\theta = \frac{1}{r} \left[\frac{1}{\sin\theta} \frac{\partial E_r}{\partial \varphi} - \frac{\partial \left(r E_\varphi \right)}{\partial r} \right], \tag{6}$$

$$-\mu \frac{\partial H_\varphi}{\partial t} - \sigma_m H_\varphi = \frac{1}{r} \left[\frac{\partial \left(r E_\theta \right)}{\partial r} - \frac{\partial E_r}{\partial \theta} \right]. \tag{7}$$

*Project supported by the National Natural Science Foundation of China (Grant Nos. 61301063 and 41305017).

†Corresponding author. E-mail: liuyawen1111@163.com

© 2014 Chinese Physical Society and IOP Publishing Ltd

It is seen that equations (2)–(7) involve only the first order derivative both in time and in space. However, by applying the Taylor series expansion to a function $f(x)$, after some simple manipulations, we can obtain $(2L)$-th-order approximation for the first-order derivation of $f(x)$

$$f'(x) \approx \frac{1}{\Delta x}\sum_{l=-L}^{L-1} a(l) f\left(x+l+\frac{1}{2}\right). \tag{8}$$

Figure 1 shows the unit cell of the HO-FDTD scheme. By replacing the first-order time derivatives in Eqs. (2)–(7) with the 2nd-order central difference approximation and the first-order spatial derivatives in Eqs. (2)–(7) with the 6th-order central difference approximation, the $(2,6)$-th-order FDTD formulas can be obtained. Taking the field E_r for example, its discretized form is described as

$$\begin{aligned}
&\varepsilon\frac{E^{r,n+1}_{i+1/2,j,k}-E^{r,n}_{i+1/2,j,k}}{\Delta t}+\sigma\frac{E^{r,n+1}_{i+1/2,j,k}+E^{r,n}_{i+1/2,j,k}}{2}\\
&=\frac{1}{(i+1/2)\Delta r\sin(j\Delta\theta)}\times\left\{\frac{1}{\Delta\theta}\sum_{l=-3}^{2}a(l)\sin[(j+l+1/2)\Delta\theta]H^{\varphi,n+1/2}_{i+1/2,j+l+1/2,k}-\frac{1}{\Delta\varphi}\sum_{l=-3}^{2}a(l)H^{\theta,n+1/2}_{i+1/2,j,k+l+1/2}\right\},
\end{aligned} \tag{9}$$

that is

$$\begin{aligned}
E^{r,n+1}_{i+1/2,j,k} &= \frac{2\varepsilon-\sigma\Delta t}{2\varepsilon+\sigma\Delta t}E^{r,n}_{i+1/2,j,k}+\frac{2\Delta t}{2\varepsilon+\sigma\Delta t}\frac{1}{(i+1/2)\Delta r\sin(j\Delta\theta)}\\
&\quad\times\left\{\frac{1}{\Delta\theta}\sum_{l=-3}^{2}a(l)\sin[(j+l+1/2)\Delta\theta]H^{\varphi,n+1/2}_{i+1/2,j+l+1/2,k}-\frac{1}{\Delta\varphi}\sum_{l=-3}^{2}a(l)H^{\theta,n+1/2}_{i+1/2,j,k+l+1/2}\right\}.
\end{aligned} \tag{10}$$

The $(2,6)$-th-order FDTD formulas of the other fields can be written as

$$\begin{aligned}
E^{\theta,n+1}_{i,j+1/2,k} &= \frac{2\varepsilon-\sigma\Delta t}{2\varepsilon+\sigma\Delta t}E^{\theta,n}_{i,j+1/2,k}+\frac{2\Delta t}{2\varepsilon+\sigma\Delta t}\frac{1}{i\Delta r}\\
&\quad\times\left\{\frac{1}{\sin[(j+1/2)\Delta\theta]\Delta\varphi}\sum_{l=-3}^{2}a(l)H^{r,n+1/2}_{i,j+1/2,k+l+1/2}-\sum_{l=-3}^{2}a(l)(i+l+1/2)H^{\varphi,n+1/2}_{i+l+1/2,j+1/2,k}\right\},
\end{aligned} \tag{11}$$

$$\begin{aligned}
E^{\varphi,n+1}_{i,j,k+1/2} &= \frac{2\varepsilon-\sigma\Delta t}{2\varepsilon+\sigma\Delta t}E^{\varphi,n}_{i,j,k+1/2}+\frac{2\Delta t}{2\varepsilon+\sigma\Delta t}\frac{1}{i\Delta r}\\
&\quad\times\left[\sum_{l=-3}^{2}a(l)(i+l+1/2)H^{\theta,n+1/2}_{i+l+1/2,j,k+1/2}-\frac{1}{\Delta\theta}\sum_{l=-3}^{2}a(l)H^{r,n+1/2}_{i,j+l+1/2,k+1/2}\right],
\end{aligned} \tag{12}$$

$$\begin{aligned}
H^{r,n+1/2}_{i,j+1/2,k+1/2} &= \frac{2\mu-\sigma_m\Delta t}{2\mu+\sigma_m\Delta t}H^{r,n-1/2}_{i,j+1/2,k+1/2}-\frac{2\Delta t}{2\mu+\sigma_m\Delta t}\frac{1}{i\Delta r\sin[(j+1/2)\Delta\theta]}\\
&\quad\times\left\{\frac{1}{\Delta\theta}\sum_{l=-3}^{2}a(l)\sin[(j+l+1)\Delta\theta]E^{\varphi,n}_{i,j+l+1,k+1/2}-\frac{1}{\Delta\varphi}\sum_{l=-3}^{2}a(l)E^{\theta,n}_{i,j+1/2,k+l+1}\right\},
\end{aligned} \tag{13}$$

$$\begin{aligned}
H^{\theta,n+1/2}_{i+1/2,j,k+1/2} &= \frac{2\mu-\sigma_m\Delta t}{2\mu+\sigma_m\Delta t}H^{\theta,n-1/2}_{i+1/2,j,k+1/2}-\frac{2\Delta t}{2\mu+\sigma_m\Delta t}\frac{1}{(i+1/2)\Delta r}\\
&\quad\times\left[\frac{1}{\sin(j\Delta\theta)\Delta\varphi}\sum_{l=-3}^{2}a(l)E^{r,n}_{i+1/2,j,k+l+1}-\sum_{l=-3}^{2}a(l)(i+l+1)E^{\varphi,n}_{i+l+1,j,k+1/2}\right],
\end{aligned} \tag{14}$$

$$\begin{aligned}
H^{\varphi,n+1/2}_{i+1/2,j+1/2,k} &= \frac{2\mu-\sigma_m\Delta t}{2\mu+\sigma_m\Delta t}H^{\varphi,n-1/2}_{i+1/2,j+1/2,k}-\frac{2\Delta t}{2\mu+\sigma_m\Delta t}\frac{1}{(i+1/2)\Delta r}\\
&\quad\times\left[\sum_{l=-3}^{2}a(l)(i+l+1)E^{\theta,n}_{i+l+1,j+1/2,k}-\frac{1}{\Delta\theta}\sum_{l=-3}^{2}a(l)E^{r,n}_{i+1/2,j+l+1,k}\right],
\end{aligned} \tag{15}$$

where $E^{\kappa,n}_{i,j,k}$ and $H^{\kappa,n}_{i,j,k}$, with $\kappa=r,\theta,\varphi$, are the corresponding field expansions. The indices i, j, k, and n represent the discrete space and time indices related to the space and time coordinates via $r=i\Delta r$, $\theta=j\Delta\theta$, $\varphi=k\Delta\varphi$, and $t=n\Delta t$, where Δr, $\Delta\theta$, $\Delta\varphi$, and Δt are the space and time discretization intervals in r, θ, φ, and t directions. The coefficients $a(l)$ are defined as follows:

$$a(l)=\frac{(-1)^l}{2(l+1/2)^2}\frac{[(2L-1)!!]^2}{(2L-2-2l)!!\,(2L+2l)!!}. \tag{16}$$

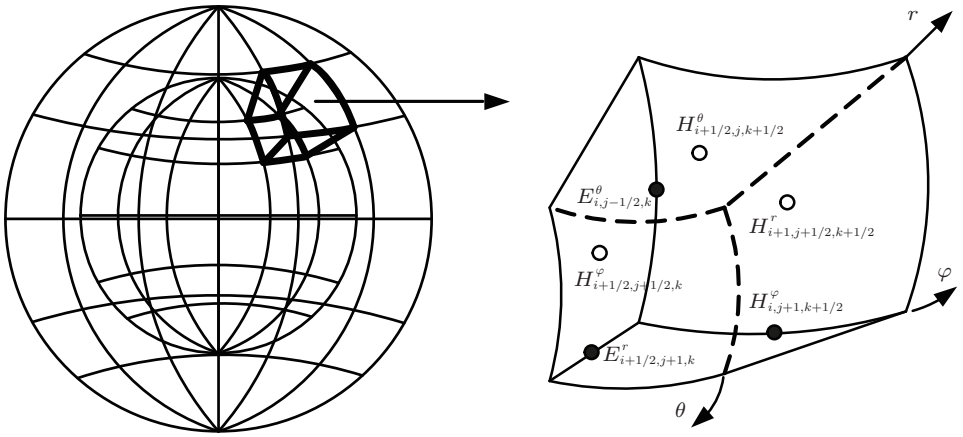


Fig. 1. A nonuniform spherical unit cell for the HO-FDTD scheme.

The coefficients for $0 \le l \le 2$ are shown in Table 1. The values of coefficient $a(l)$ for $l < 0$ are given by the symmetry relation $a(-1-l) = -a(l)$.

Table 1. Values of coefficient $a(l)$ for $0 \le l \le 2$.

l	$a(l)$
0	1.171875000
1	−0.065104167
2	0.004687500

As can be seen in Fig. 2, where we assume that the total meshes are $N_r \times (N_\theta + 1) \times (N_\varphi + 1)$, because of the characteristic of the field components in the HO-FDTD algorithm, at the points $i = 0,1,2$ or $j = 0,1,2,N_\theta - 2,N_\theta - 1,N_\theta$ or $k = 0,1,2,N_\varphi - 2,N_\varphi - 1,N_\varphi$, some of the $\boldsymbol{E}$ and $\boldsymbol{H}$ fields need to be disposed particularly.

Firstly, observing Eq. (10), it is noted that when $j = 0$ or N_θ, the E_r value is singular, and this problem can be solved by using the Ampere's law[18]

$$\oint_L \boldsymbol{H} \cdot \mathrm{d}\boldsymbol{l} = \iint_s \left(\varepsilon \frac{\partial}{\partial t} \boldsymbol{E} + \sigma \boldsymbol{E} \right) \cdot \mathrm{d}\boldsymbol{s} \tag{17}$$

where the contour L is the circle defined by $j = 1/2$ or $N_\theta - 1/2$. Taking the integral of expression (17), we can obtain the formula for updating E_r at $j = 0$

$$E^{r,\,n+1}_{i+1/2,0,k} = \frac{2\varepsilon - \sigma\Delta t}{2\varepsilon + \sigma\Delta t} E^{r,\,n}_{i+1/2,0,k} + \frac{\sin(\Delta\theta/2)\,\Delta\varphi\Delta t}{(2\varepsilon + \sigma\Delta t)\,(i+1/2)\,\Delta r\,[1-\cos(\Delta\theta/2)]\,\pi} \times \sum_j H^{\varphi,n+1/2}_{i+1/2,1/2,k}. \tag{18}$$

At $j = N_\theta$, the formula is

$$E^{r,\,n+1}_{i+1/2,N_\theta,k} = \frac{2\varepsilon - \sigma\Delta t}{2\varepsilon + \sigma\Delta t} E^{r,\,n}_{i+1/2,N_\theta,k} - \frac{\sin(\Delta\theta/2)\,\Delta\varphi\Delta t}{(2\varepsilon + \sigma\Delta t)\,(i+1/2)\,\Delta r\,[1-\cos(\Delta\theta/2)]\,\pi} \times \sum_j H^{\varphi,n+1/2}_{i+1/2,N_\theta-1/2,k}. \tag{19}$$

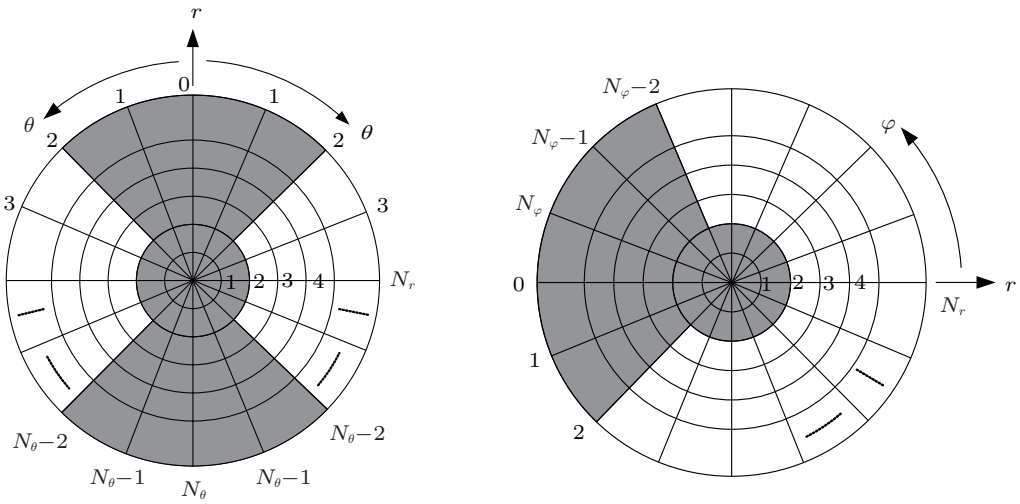


Fig. 2. Areas need to be particularly treated (dark parts). (a) The r–θ plane. (b) The r–φ plane.

Moreover, when $j=1,2,N_\theta-2,N_\theta-1,N_\theta$ or $k=0,1,2,N_\varphi-2,N_\varphi-1,N_\varphi$ and E_r should be treated particularly. Taking the spatial point $((i+1/2)\Delta r,\Delta\theta,0)$ for example, the updated equation of E_r is

$$E^{r,n+1}_{i+1/2,1,0}=\frac{2\varepsilon-\sigma\Delta t}{2\varepsilon+\sigma\Delta t}E^{r,n}_{i+1/2,1,0}+\frac{2\Delta t}{2\varepsilon+\sigma\Delta t}\frac{1}{(i+1/2)\Delta r\sin(\Delta\theta)}\left\{\frac{1}{\Delta\theta}\left[\begin{array}{l}a(0)\left(\sin((1+0+1/2)\Delta\theta)H^{\varphi,n+1/2}_{i+1/2,1+0+1/2,0}\right.\\ \left.-\sin((1-1+1/2)\Delta\theta)H^{\varphi,n+1/2}_{i+1/2,1-1+1/2,0}\right)\\ +a(1)\left(\sin((1+1+1/2)\Delta\theta)H^{\varphi,n+1/2}_{i+1/2,1+1+1/2,0}\right.\\ \left.+\sin((1-2+1/2)\Delta\theta)H^{\varphi,n+1/2}_{i+1/2,-(1-2+1/2),N_\varphi/2}\right)\\ +a(2)\left(\sin((1+2+1/2)\Delta\theta)H^{\varphi,n+1/2}_{i+1/2,1+2,0}\right.\\ \left.+\sin((1-3+1/2)\Delta\theta)H^{\varphi,n+1/2}_{i+1/2,-(1-3+1/2),N_\varphi/2}\right)\end{array}\right]\right.$$

$$\left.-\frac{1}{\Delta\varphi}\left[\begin{array}{l}a(0)\left(H^{\theta,n+1/2}_{i+1/2,1,0+1/2}-H^{\theta,n+1/2}_{i+1/2,1,N_\varphi+1/2}\right)\\ +a(1)\left(H^{\theta,n+1/2}_{i+1/2,1,1+1/2}-H^{\theta,n+1/2}_{i+1/2,1,N_\varphi-1/2}\right)\\ +a(2)\left(H^{\theta,n+1/2}_{i+1/2,1,2+1/2}-H^{\theta,n+1/2}_{i+1/2,1,N_\varphi-3/2}\right)\end{array}\right]\right\},\tag{20}$$

that is,

$$\begin{aligned}E^{r,n+1}_{i+1/2,1,0}=&\frac{2\varepsilon-\sigma\Delta t}{2\varepsilon+\sigma\Delta t}E^{r,n}_{i+1/2,1,0}+\frac{2\Delta t}{2\varepsilon+\sigma\Delta t}\frac{1}{(i+1/2)\Delta r\sin(\Delta\theta)}\\&\times\left\{\frac{1}{\Delta\theta}\left[\begin{array}{l}a(0)\left(\sin\left(\frac{3}{2}\Delta\theta\right)H^{\varphi,n+1/2}_{i+1/2,3/2,0}-\sin\left(\frac{1}{2}\Delta\theta\right)H^{\varphi,n+1/2}_{i+1/2,1/2,0}\right)\\ +a(1)\left(\sin\left(\frac{5}{2}\Delta\theta\right)H^{\varphi,n+1/2}_{i+1/2,5/2,0}-\sin\left(\frac{1}{2}\Delta\theta\right)H^{\varphi,n+1/2}_{i+1/2,1/2,N_\varphi/2}\right)\\ +a(2)\left(\sin\left(\frac{7}{2}\Delta\theta\right)H^{\varphi,n+1/2}_{i+1/2,7/2,0}-\sin\left(\frac{3}{2}\Delta\theta\right)H^{\varphi,n+1/2}_{i+1/2,3/2,N_\varphi/2}\right)\end{array}\right]\right.\\&\left.-\frac{1}{\Delta\varphi}\left[\begin{array}{l}a(0)\left(H^{\theta,n+1/2}_{i+1/2,1,1/2}-H^{\theta,n+1/2}_{i+1/2,1,N_\varphi+1/2}\right)\\ +a(1)\left(H^{\theta,n+1/2}_{i+1/2,1,3/2}-H^{\theta,n+1/2}_{i+1/2,1,N_\varphi-1/2}\right)\\ +a(2)\left(H^{\theta,n+1/2}_{i+1/2,1,5/2}-H^{\theta,n+1/2}_{i+1/2,1,N_\varphi-3/2}\right)\end{array}\right]\right\}.\end{aligned}\tag{21}$$

Next, observing Eq. (11), it can also be seen that the value of E_θ is singular at $i=0$. A simple method to treat this problem is to let $E_\theta=0$, which is feasible if the origin of the coordinate system is occupied by a perfect conductor. Another possible way is to transform the E_θ fields at $i=0$ into Cartesian coordinates, and then transform back to spherical coordinates.

Furthermore, when $i=1,2$ or $k=0,1,2,N_\varphi-2,N_\varphi-1$, the N_φ and E_θ should be treated particularly. Taking the spatial point $(\Delta r,(j+1/2)\Delta\theta,0)$ for example, the updated equation of E_θ is

$$E^{\theta,n+1}_{1,j+1/2,0}=\frac{2\varepsilon-\sigma\Delta t}{2\varepsilon+\sigma\Delta t}E^{\theta,n}_{1,j+1/2,0}+\frac{2\Delta t}{2\varepsilon+\sigma\Delta t}\frac{1}{\Delta r}\left\{\frac{1}{\sin[(j+1/2)\Delta\theta]\Delta\varphi}\left[\begin{array}{l}a(0)\left(H^{r,n+1/2}_{1,j+1/2,1/2}-H^{r,n+1/2}_{1,j+1/2,N_\varphi+1/2}\right)\\ +a(1)\left(H^{r,n+1/2}_{1,j+1/2,3/2}-H^{r,n+1/2}_{1,j+1/2,N_\varphi-1/2}\right)\\ +a(2)\left(H^{r,n+1/2}_{1,j+1/2,5/2}-H^{r,n+1/2}_{1,j+1/2,N_\varphi-3/2}\right)\end{array}\right]\right.$$

$$\left.-\left[\begin{array}{l}a(0)\left(\frac{3}{2}H^{\varphi,n+1/2}_{3/2,j+1/2,0}-\frac{1}{2}H^{\varphi,n+1/2}_{1/2,j+1/2,0}\right)\\ +a(1)\left(\frac{5}{2}H^{\varphi,n+1/2}_{5/2,j+1/2,0}-\frac{3}{2}H^{\varphi,n+1/2}_{1/2,j+1/2,N_\varphi}\right)\\ +a(2)\left(\frac{7}{2}H^{\varphi,n+1/2}_{7/2,j+1/2,0}-\frac{5}{2}H^{\varphi,n+1/2}_{5/2,j+1/2,N_\varphi}\right)\end{array}\right]\right\}.\tag{22}$$

Referring to Eq. (12), the treatment of E_φ at $i=0$ or $j=0$, N_θ is the same as that of E_θ, and when $i=1,2$ or $j=1$, 2, $N_\theta-2$, $N_\theta-1$, the E_θ should also be treated particularly. Taking the spatial point $(\Delta r, \Delta\theta, (k+1/2)\Delta\varphi)$ for example, the updated equation of E_φ is

$$E^{\varphi,n+1}_{1,1,k+1/2} = \frac{2\varepsilon-\sigma\Delta t}{2\varepsilon+\sigma\Delta t}E^{\varphi,n}_{1,1,k+1/2} + \frac{2\Delta t}{2\varepsilon+\sigma\Delta t}\frac{1}{\Delta r}\left\{\begin{bmatrix} a(0)\left(\frac{3}{2}H^{\theta,n+1/2}_{3/2,1,k+1/2}-\frac{1}{2}H^{\theta,n+1/2}_{1/2,1,k+1/2}\right) \\ +a(1)\left(\frac{5}{2}H^{\theta,n+1/2}_{5/2,1,k+1/2}-\frac{1}{2}H^{\theta,n+1/2}_{1/2,1,k+1/2-N_\varphi/2}\right) \\ +a(2)\left(\frac{7}{2}H^{\theta,n+1/2}_{7/2,1,k+1/2}-\frac{3}{2}H^{\theta,n+1/2}_{3/2,1,k+1/2-N_\varphi/2}\right)\end{bmatrix}\right.$$
$$\left.-\frac{1}{\Delta\theta}\begin{bmatrix} a(0)\left(H^{r,n+1/2}_{1,3/2,k+1/2}-H^{r,n+1/2}_{1,1/2,k+1/2}\right) \\ +a(1)\left(H^{r,n+1/2}_{1,5/2,k+1/2}-H^{r,n+1/2}_{1,1/2,k+1/2-N_\varphi/2}\right) \\ +a(2)\left(H^{r,n+1/2}_{1,7/2,k+1/2}-H^{r,n+1/2}_{1,3/2,k+1/2-N_\varphi/2}\right)\end{bmatrix}\right\}. \tag{23}$$

The treatment of the $\boldsymbol{H}$ fields at the proposed special points is similar to that of the $\boldsymbol{E}$ fields, and can be obtained by duality.

3. Stability and dispersion analysis

3.1. Stability analysis

Using the normalized value of the vector of the magnetic fields ($\sqrt{\mu/\varepsilon}\boldsymbol{H}\to\boldsymbol{H}$), equation (1) can be rewritten as

$$\nabla\times\boldsymbol{E} = -\frac{1}{c}\frac{\partial\boldsymbol{H}}{\partial t},\quad \nabla\times\boldsymbol{H} = \frac{1}{c}\frac{\partial E}{\partial t}, \tag{24}$$
$$c = \frac{1}{\mu\varepsilon}.$$

Defining that $\boldsymbol{V}=\boldsymbol{H}+\mathrm{j}\boldsymbol{E}$, then we can obtain

$$\mathrm{j}\nabla\times\boldsymbol{V} = \frac{1}{c}\frac{\partial\boldsymbol{V}}{\partial t}. \tag{25}$$

Considering the following eigenvalue problem:

$$\frac{\partial\boldsymbol{V}}{\partial t} = \lambda\boldsymbol{V}, \tag{26}$$
$$\mathrm{j}c\nabla\times\boldsymbol{V} = \lambda\boldsymbol{V}. \tag{27}$$

The finite-difference approximations of the time derivatives on the left-hand side of Eq. (26) can be written as

$$\frac{\boldsymbol{V}^{n+1/2}-\boldsymbol{V}^{n-1/2}}{\Delta t} = \lambda\boldsymbol{V}^n. \tag{28}$$

To maintain the stability during normal time stepping, the imaginary part of λ, $\mathrm{Im}(\lambda)$, must satisfy

$$|\mathrm{Im}(\lambda)| \le \frac{2}{\Delta t}. \tag{29}$$

Assuming that the calculating space medium is homogeneous, lossless, and non-magnetic, any monochromatic plane wave can be indicated by

$$V_{I,J,K} = V_0\exp[-\mathrm{j}(k_rI\Delta r + k_\theta\Delta rJ\Delta\theta + k_\varphi I\Delta r\sin(J\Delta\theta)K\Delta\varphi)]. \tag{30}$$

Substituting Eq. (30) into Eq. (28) and applying Euler's identity, then we can obtain

$$\lambda^2 = \left\{\frac{1}{\Delta r}\left[\sum_{i'=0}^{2}a(i')\sin\left(k_r\Delta r\left(i'+\frac{1}{2}\right)\right)\right]\right\}^2 + \left\{\frac{1}{r'\Delta\theta}\left[\sum_{j'=0}^{2}a(j')\sin\left(k_\theta r'\left(j'+\frac{1}{2}\right)\Delta\theta\right)\right]\right\}^2$$
$$+\left\{\frac{1}{r'\Delta\varphi\sin\Delta\theta}\left[\sum_{k'=0}^{2}a(k')\sin\left(k_\varphi r'\Delta\varphi\left(k'+\frac{1}{2}\right)\times\sin\Delta\theta\right)\right]\right\}^2. \tag{31}$$

In Eq. (31), r' is the radial location, λ is a pure imaginary that is bounded for any wave vector $k=(k_r,k_\theta,k_\varphi)$

$$|\mathrm{Im}(\lambda)| \le 2c\left(\sum_{i'=0}^{2}a(i')\right)\left(\frac{1}{(\Delta r)^2}+\frac{4}{(\Delta r\Delta\theta)^2}+\frac{4}{(\Delta r\Delta\varphi\sin\Delta\theta)^2}\right)^{1/2}, \tag{32}$$

where $c=1/\sqrt{\mu\varepsilon}$ is the velocity of light.

In order to maintain that the numerical stability remains for any spatial mode, the upper bound of expression (32) must be smaller than or equal to Eq. (29), that is

$$\Delta t \le \frac{S}{c\sqrt{\frac{1}{\Delta r^2}+\frac{4}{(\Delta r\Delta\theta)^2}+\frac{4}{(\Delta r\Delta\varphi\sin\Delta\theta)^2}}}, \tag{33}$$

where

$$S = \frac{1}{\left[\sum_{i'=0}^{2}a(i')\right]} \approx 0.8727. \tag{34}$$

It is known that

$$\Delta t_{\mathrm{FDTD}} \leq \frac{1}{c\sqrt{\dfrac{1}{(\Delta r)^2}+\dfrac{4}{(\Delta r\Delta\theta)^2}+\dfrac{4}{(\Delta r\Delta\varphi\sin\Delta\theta)^2}}}. \quad (35)$$

Equations (33)–(35) show that for the same discretization size, the upper bounds of the time steps of HO-FDTD and FDTD are comparable and related through the factor S.

3.2. Dispersion analysis

The numerical dispersion errors of the standard HO-FDTD, standard FDTD, and MRTD are investigated in this section. By substituting a time-harmonic trial solution into the update equations and numerically solving the resulting nonlinear equation, the dispersion relation can be obtained as[14]

$$\begin{aligned}&\left[\frac{1}{c\Delta t}\sin\left(\frac{\omega\Delta t}{2}\right)\right]^2\\ &=\left\{\frac{1}{\Delta r}\left[\sum_{i'=0}^{2}a\left(i'\right)\sin\left(k_r\left(i'+\frac{1}{2}\right)\Delta r\right)\right]\right\}^2\\ &+\left\{\frac{1}{r'\Delta\theta}\left[\sum_{j'=0}^{2}a\left(j'\right)\sin\left(k_\theta r'\left(j'+\frac{1}{2}\right)\Delta\theta\right)\right]\right\}^2\\ &+\left\{\frac{1}{r'\Delta\varphi\sin\Delta\theta}\left[\sum_{k'=0}^{2}a\left(k'\right)\sin\left(k_\varphi r'\Delta\varphi\left(k'+\frac{1}{2}\right)\right.\right.\right.\\ &\left.\left.\left.\times\sin\Delta\theta\right)\right]\right\}^2, \end{aligned} \quad (36)$$

where ω is the wave angular frequency, ρ' is the radial location, and $k_{r,\theta,\varphi}$ is the ρ, θ, φ components of the numerical wave vector respectively. It is obvious that it is difficult to treat the three-dimensional (3D) dispersion problem, so for simplicity, a two-dimensional (2D) problem in the θ–φ plane is analyzed. Defining that the Courant–Friedrichs–Lewy number (CFLN) $c\Delta t/\delta = p$ and $r'\Delta\theta = r'\Delta\varphi\sin\Delta\theta = \delta$, equation (36) can be rewritten as

$$\begin{aligned}&\omega\Delta t\\ &=2\arcsin\left\{p\sqrt{\begin{aligned}&\left[\sum_{j'=0}^{2}a\left(j'\right)\sin\left(k_\varphi\delta\left(j'+\frac{1}{2}\right)\right)\right]^2\\ &+\left[\sum_{k'=0}^{2}a\left(k'\right)\sin\left(k_z\delta\left(k'+\frac{1}{2}\right)\right)\right]^2\end{aligned}}\right\}.\end{aligned} \quad (37)$$

To permit the determination of $\boldsymbol{k}$ for any wave-propagation direction, we define that

$$\boldsymbol{k} = \left(k_\varphi, k_z\right) = k_0\left(\cos\alpha, \sin\alpha\right),$$

where α represents the azimuth angle in polar coordinates. Since $k_0 = \omega/v_p = 2\pi/\lambda_0$, where v_p represents the numerical phase velocity and λ_0 denotes the free-space wavelength, equation (37) can be rewritten as

$$\frac{v_p}{c} = \frac{N}{\pi}\frac{1}{p}\arcsin\left\{p\sqrt{\begin{aligned}&\left[\sum_{j'=0}^{2}a\left(j'\right)\sin\left(\frac{2\pi}{N}\cos\alpha\left(j'+\frac{1}{2}\right)\right)\right]^2\\ &+\left[\sum_{k'=0}^{2}a\left(k'\right)\sin\left(\frac{2\pi}{N}\sin\alpha\left(k'+\frac{1}{2}\right)\right)\right]^2\end{aligned}}\right\}, \quad (38)$$

where $N = \lambda_0/\delta$ is the grid-sampling density. To satisfy the stability requirements, p must be smaller than 0.6362 ($= 0.8997/\sqrt{2}, \Delta\varphi = 2\Delta z/\Delta\rho$) for the 2D simulations.

Figures 3(a) and 3(b) show the dispersion errors versus N with CFLN = 0.125 and $\alpha = 0°$, 45°, figures 3(c) and 3(d) show the dispersion errors versus N with CFLN = 0.3 and $\alpha = 0°$, 45°. From these figures, it is obvious that the dispersion errors for both HO-FDTD and MRTD are far lower than for FDTD. The dispersion error for HO-FDTD is generally lower than for MRTD. When the grid-sampling density is very low ($N = 2$ to 3), the dispersion error for MRTD is lower than for HO-FDTD, but the spatial sampling rates for MRTD are so low that it generally precludes practical use. Moreover, it can also be concluded that the advantage of HO-FDTD becomes much more obvious as the CFLN decreases.

Figure 4 describes the variations of v_p in HO-FDTD and MRTD approaches versus propagation direction α with a value of $p = 0.125$. In Fig. 4(a), two different values of grid-sampling density λ_0/δ, namely, the values of N, are examined for HO-FDTD and MRTD: $N = 2$ points per λ_0 and $N = 3$, and three for HO-FDTD and MRTD in Fig. 4(b): $\lambda_0/\delta = 4$, $\lambda_0/\delta = 5$, and $\lambda_0/\delta = 6$. From this figure, it can be easily seen that the propagation speed of v_p is slower than the speed of light for the HO-FDTD scheme, but is faster than the speed of light for the MRTD scheme. We can also see an interesting phenomenon that the curves for both HO-FDTD and MRTD are symmetrical with respect to $\alpha = 45°$; for the HO-FDTD approach, the numerical phase velocity becomes faster and faster gradually, and then becomes slower and slower gradually; for the MRTD approach, the variation of v_p is similar to that for the HO-FDTD in Fig. 4(a), but the MRTD can keep a higher accuracy with the same grid-sampling density than the HO-FDTD, which validates the conclusion above; in Fig. 4(b), the variation of v_p for MRTD is opposite

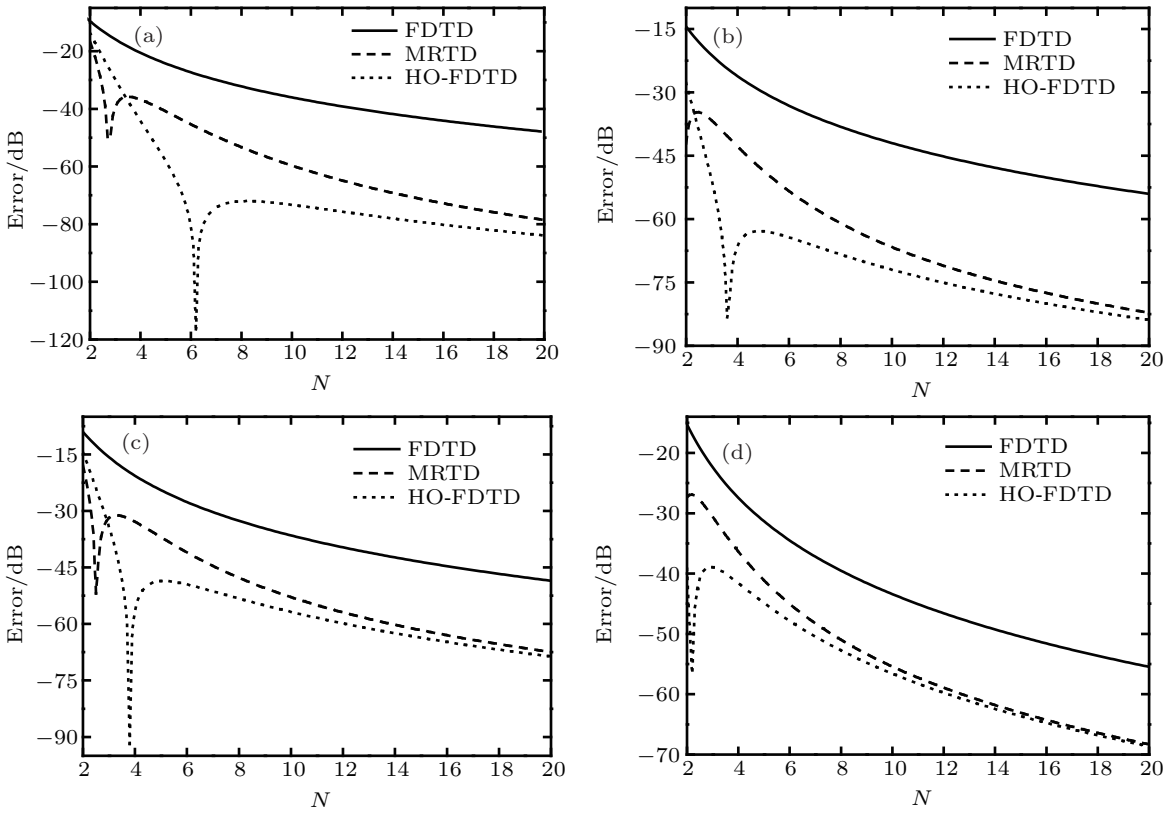


Fig. 3. Dispersion errors versus N for FDTD, HO-FDTD, and MRTD methods. (a) CFLN = 0.125 and $\alpha = 0°$; (b) CFLN = 0.125 and $\alpha = 45°$; (c) CFLN = 0.3 and $\alpha = 0°$; (d) CFLN = 0.3 and $\alpha = 45°$.

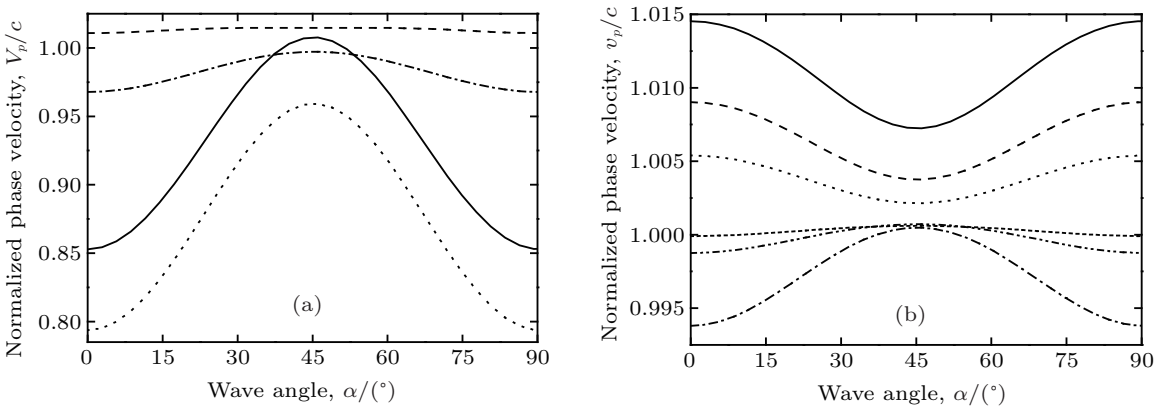


Fig. 4. Variations of v_p/c with wave-propagation angle for 2D HO-FDTD and MRTD grids. In panel (a) solid line for $N = 2$, MRTD; dashed line for $N = 3$, MRTD; dotted line for $N = 2$, Ho-FDTD; and dash–dot line for $N = 3$, HO-FDTD. In panel (b) solid line for $N = 4$, MRTD; thicker dashed line for $N = 5$, MRTD; dotted line for $N = 6$, MRTD; dash–dot line for $N = 4$, HO-FDTD; dash–dot–dot–dash line for $N = 5$, HO–FDTD; thiner dashed line for $N = 6$, HO-FDTD.

to the HO-FDTD: v_p firstly becomes slower and slower gradually, and then becomes faster and faster gradually, v_p is slowest at $\alpha = 45°$, and it is obvious that the HO-FDTD can keep a higher accuracy with the same grid-sampling density than the MRTD. Since the spatial stencil of the proposed HO-FDTD and MRTD is larger than that of the FDTD, and the proposed spatial sampling rate is too low for FDTD, for simplicity, the curves for FDTD are not illustrated here.

To demonstrate the benefits of the high linear dispersion characteristics of the HO-FDTD scheme, as Table 2 shows, the simulations results of the resonant frequencies for an air-filled spherical resonator are given here. The radius of the cavity resonator is $r = 1$ m, and the constitutive parameters for air can be defined as $\sigma = 0$, $\sigma_m = 0$, and $\varepsilon = 8.85 \times 10^{-12}$ F/m, $\mu = 4\pi \times 10^{-7}$ H/m. Its fundamental-mode frequency is 131.01 GHz. In the simulation using FDTD scheme, the computation domain is discretized using the grid with $\Delta\rho = 3.125$ cm, $\Delta\theta = \pi/48$, and $\Delta\varphi = \pi/24$, leading to a mesh of $32 \times 48 \times 48$ grid points. For the MRTD and HO-FDTD scheme, a grid with $\Delta\rho = 12.5$ cm, $\Delta\theta = \pi/6$, $\Delta\varphi = \pi/6$ and with a mesh of $8 \times 6 \times 12$ grid points, is chosen. Note that the time discretization interval $\Delta t_{\mathrm{FDTD}} = 4.421 \times 10^{-13}$ s, $\Delta t_{\mathrm{MRTD}} = \Delta t_{\mathrm{HO-FDTD}} = 1.454 \times 10^{-11}$ s are chosen for the

three schemes. The source is a Gaussian pulse applied to the E_z component located at the grid point (3, 3, 0) and given as

$$E^{\varphi,n+1}_{3,3+1/2,0} = E^{\varphi,n}_{3,3+1/2,0} - \exp\left[-4\pi\left(t-t_0\right)/\tau\right]^2, \quad (39)$$

where $t_0 = \tau = 0.2$ ns. Compared with the case using the FDTD method, the total number of grid points is reduced by a factor of 64, and the execution time for the analysis is reduced by a factor of 25 for MRTD and HO-FDTD methods. Moreover, it is seen that for the MRTD method, the relative error of the resonant frequencies is positive, and for the FDTD and HO-FDTD methods, the relative errors of the resonant frequencies are negative, which can be expected from the dispersion diagrams, see Fig. 4. Figure 5 depicts the normalized magnitude of the E_r in time and frequency domain calculated by HO-FDTD at the grid point (5, 3, 4).

Table 2. Simulation results.

Scheme	FDTD	MRTD	HO-FDTD
Results /GHz	130.761	131.130	131.008
Relative error	−0.190%	0.092%	−0.002%
Mesh size	$32\times48\times48$	$8\times6\times12$	$8\times6\times12$
No. of iterations	65536	65536	65536
CPU time/s	512.86	20.83	20.10

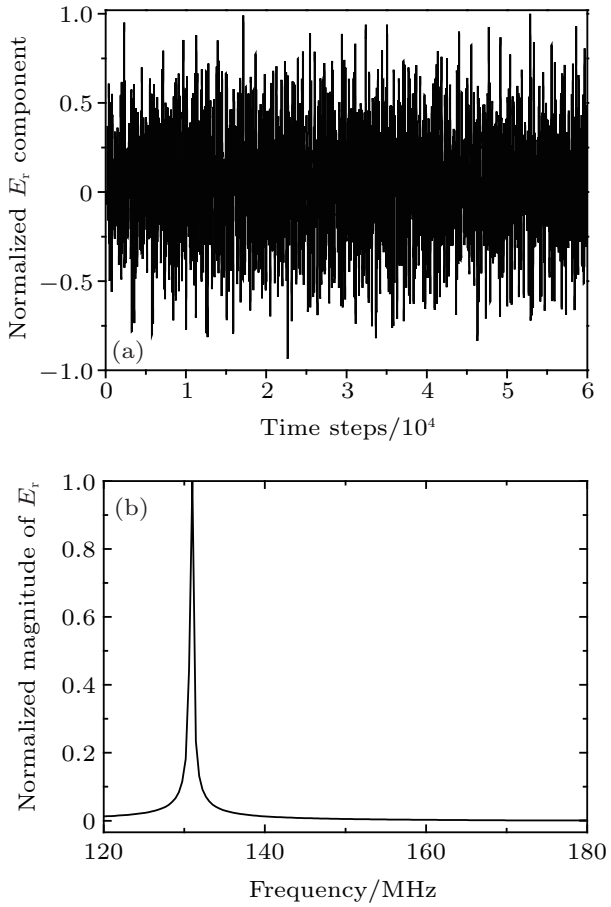


Fig. 5. Normalized magnitude of the E_r field in time and frequency domain.

In this work, the spherical resonator is a kind of perfect electric conductor (PEC) shielded structure. Since the HO-FDTD scheme does not allow localized boundary conditions, as figure 6 shows, the image technique is applied to the PEC boundary.[19]

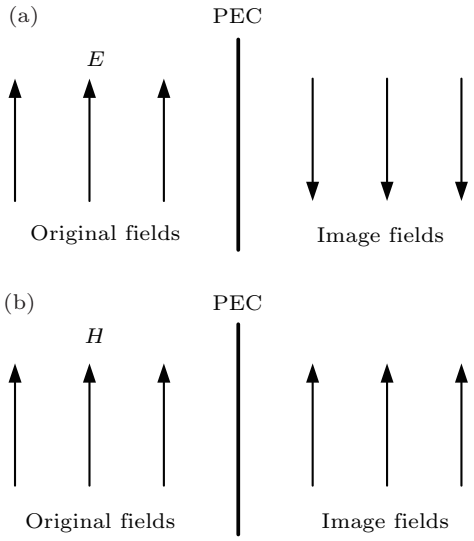


Fig. 6. Original and image fields of the HO-FDTD lattice with respect to PEC boundary.

4. Implementation of the PML

In the spherical coordinate system, the PML formulations are posed in the stretched coordinate space,[20] i.e.,

$$\mathrm{j}\omega\varepsilon_0 E_r = \frac{1}{\tilde{r}\sin\theta}\left[\frac{\partial\left(\sin\theta H_\varphi\right)}{\partial\theta} - \frac{\partial H_\theta}{\partial\varphi}\right], \quad (40)$$

$$\mathrm{j}\omega\varepsilon_0 \tilde{E}_\theta = \frac{1}{s_r}\left[\frac{1}{\sin\theta}\frac{\partial\tilde{H}_r}{\partial\varphi} - \frac{\partial\tilde{H}_\varphi}{\partial r}\right], \quad (41)$$

$$\mathrm{j}\omega\varepsilon_0 \tilde{E}_\varphi = \frac{1}{s_r}\left[\frac{\partial\tilde{H}_\theta}{r} - \frac{\partial\tilde{H}_r}{\partial\theta}\right], \quad (42)$$

$$-\mathrm{j}\omega\mu_0 H_r = \frac{1}{\tilde{r}\sin\theta}\left[\frac{\partial\left(\sin\theta E_\varphi\right)}{\partial\theta} - \frac{\partial E_\theta}{\partial\varphi}\right], \quad (43)$$

$$-\mathrm{j}\omega\mu_0 \tilde{H}_\theta = \frac{1}{s_r}\left[\frac{1}{\sin\theta}\frac{\partial\tilde{E}_r}{\partial\varphi} - \frac{\partial\tilde{E}_\varphi}{\partial r}\right], \quad (44)$$

$$-\mathrm{j}\omega\mu_0 \tilde{H}_\varphi = \frac{1}{s_r}\left[\frac{\partial\tilde{E}_\theta}{\partial r} - \frac{\partial\tilde{E}_r}{\partial\theta}\right], \quad (45)$$

$$s_r E_r = \tilde{E}_r, \quad (46)$$

$$\tilde{r}E_\theta = \tilde{E}_\theta, \quad (47)$$

$$\tilde{r}E_\varphi = \tilde{E}_\varphi, \quad (48)$$

$$s_r H_r = \tilde{H}_r, \quad (49)$$

$$\tilde{r}H_\theta = \tilde{H}_\theta, \quad (50)$$

$$\tilde{r}H_\varphi = \tilde{H}_\varphi, \quad (51)$$

where s_r is the stretched-coordinate metric, which is assumed to be

$$s_r = 1 + \frac{\sigma^r_E}{\mathrm{j}\omega\varepsilon_0} = 1 + \frac{\sigma^r_H}{\mathrm{j}\omega\mu_0}, \quad (52)$$

and $\tilde{r}$ can be defined as

$$\begin{aligned}\tilde{r} &= \int_0^{\rho} s_r(r')\,\mathrm{d}r' \\ &= \int_0^{r}\left[1+\frac{\sigma_E(r')}{\mathrm{j}\omega\varepsilon_0}\right]\mathrm{d}r' \\ &= \int_0^{r}\left[1+\frac{\sigma_H(r')}{\mathrm{j}\omega\mu_0}\right]\mathrm{d}r'. \end{aligned} \tag{53}$$

Since the PML is achieved through complex stretching on the radial variable r, only, it is not necessary to split the fields at all in spherical coordinates. Following the procedure in Section 2, the discrete PML equations can be easily obtained (not shown here for space-saving purposes).

5. Numerical results

5.1. Validation of convergence

In this section, a 3D spherical problem in free space is discussed to validate the convergence of the PML. The cell discretization size is defined as being uniform in the r direction $\Delta r = 6$ cm. Eight-cell-thick PML layers terminate the space in the r direction, which leads to an $N_r \times N_\theta \times N_\varphi = 38 \times 16 \times 20$ cell lattice. The PML region is terminated with a PEC wall. The source is applied to the electric field component E_θ located at the grid point (5, 12, 0) as follows:

$$\begin{aligned} &E^{\theta,n+1}_{5,12+1/2,0} \\ &= E^{\theta,n}_{5,12+1/2,0} - \frac{\Delta t}{25\varepsilon_0\Delta r^3\Delta\theta\Delta\varphi\sin(12.5\Delta\theta)}\left(\frac{\mathrm{d}p}{\mathrm{d}t}\right)^{n+1/2}, \end{aligned} \tag{54}$$

where $p(t) = 10^{-10}\exp[-(t-3T)/T]^2$, with $T = 1.5$ ns. A receiver is located at the grid point (7, 6, 10). Figure 7 shows that the analytical curve and the numerical result of the PML are in good agreement, and little reflection from the PML region can be seen. It should be noted that the source–receiver positioning is such that the pulse passes through the $\theta = 0$ axis, which verifies the accuracy and stability of the spherical HO-FDTD algorithm in our discretization scheme.

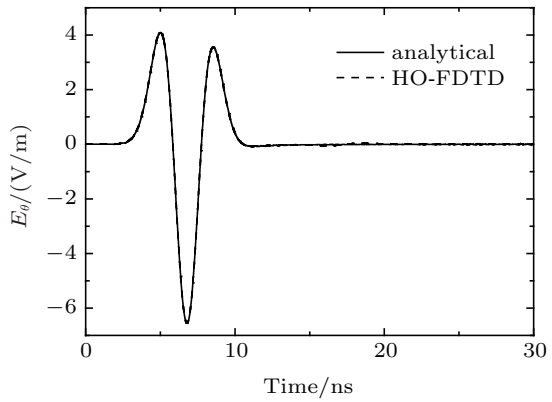


Fig. 7. Comparison between analytical and numerical results for the PML schemes in spherical coordinates.

5.2. Validation of symmetry

The computational space now is the same as before, but the excitation source is defined as

$$\begin{aligned} E^{\theta,n+1}_{6,0:N_\theta-1/2,0:N_\varphi} &= E^{\theta,n}_{6,0:N_\theta-1/2,0:N_\varphi} \\ &\quad - \exp[-(n\Delta t - 3T)/T]^2, \end{aligned} \tag{55}$$

where $T = 1.5$ ns. As figure 8 shows, in order to analyze the symmetry of the PML scheme, some sampling points are set on the circles that are vertical with $j = 0$, N_θ, and the field values at the sampling points are computed. In Fig. 8, $r = 14$ spaces, since the sampling points have the same distances from the excitation source, and are absolutely symmetrical, the computed field values should be identical.

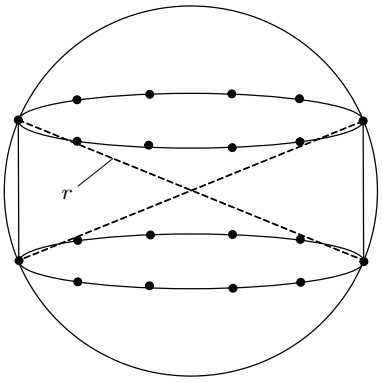


Fig. 8. Distribution of the sampling points.

The computational results are listed in Table 3. The values in lines 1 and 2 in the table are the E_θ values at the sampling points in the upper circle, and the values in lines 3 and 4 in the table are the E_θ values in the nether circle, all the values are extracted after 7000 time steps. From Table 3, it can be easily concluded that the symmetry of the PML scheme is quite good. Because the dispersion effects are different in different wave-propagation directions, the values in the table are not exactly the same. However, the error is just about 0.0003%, which is small enough to be overlooked.

Table 3. Validations of symmetry.

–2.293535	–2.293535	–2.293535	–2.293535	–2.293535
–2.293535	–2.293535	–2.293535	–2.293535	–2.293535
–2.293541	–2.293541	–2.293541	–2.293541	–2.293541
–2.293541	–2.293541	–2.293541	–2.293541	–2.293541

5.3. Dipole and conductive sphere

In this subsection, a much stronger demand of an electric dipole near a conductive sphere is considered.[21] As shown in Fig. 9, a sphere of radius $r_0 = 0.4$ m is used here. The computational domain is discretized using an $N_r \times N_\theta \times N_\varphi =$

$38 \times 18 \times 36$ cell lattice with eight-cell-thick PML terminating the grid in the r direction. The computational volume is discretized with $\Delta r = 0.1$ m and

$$\Delta\theta = \Delta\varphi = \pi/18,$$

and the time resolution is $\Delta t = 16.67$ ps. The electric dipole is located at the grid point (5, 9, 0), and is characterized by

$$P(t) = \sin(\omega t), \tag{56}$$

where

$$\omega = 2\pi f,$$

with $f = 0.5$ GHz, giving a wavelength $\lambda = 0.6$ m. It is easily demonstrated that such a dipole produces an electric field in time domain as follows:

$$E(\boldsymbol{r},t) = \frac{\mu_0}{4\pi r}\left\{\boldsymbol{e}_r\left[\frac{c}{r}\frac{\partial}{\partial t}+\frac{c^2}{r^2}\right]2\cos\theta + \boldsymbol{e}_\theta\left[\frac{\partial^2}{\partial t^2}+\frac{c}{r}\frac{\partial}{\partial t}+\frac{c^2}{r^2}\right]\sin\theta\right\}P\left(t-\frac{c}{r}\right), \tag{57}$$

and the electric dipole source can be employed in the HO-FDTD as follows:

$$E^{\theta,n+1}_{5,9+1/2,0} = E^{\theta,n}_{5,9+1/2,0} - \frac{\Delta t}{25\varepsilon_0\Delta r^3\Delta\theta\Delta\varphi\sin(9.5\Delta\theta)}\left(\frac{\mathrm{d}P}{\mathrm{d}t}\right)^{n+1/2}. \tag{58}$$

Simulations are allowed to be performed using 2500 time steps. Figures 10(a) and 10(b) show the analytical and numerical results for E_θ with $0 \le \theta \le \pi$, $\varphi = 0$. The solutions are shown only for the 10–30 radial steps to avoid larger nearer-field wave amplitudes swamping out further-field amplitudes. It is seen that the analytical and numerical results accord with each other quite well, which also validates the efficacy of the PML.

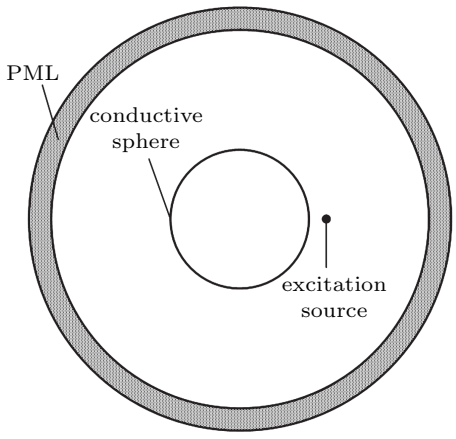


Fig. 9. The r–φ-plane of the computational model ($\theta = \pi/2$).

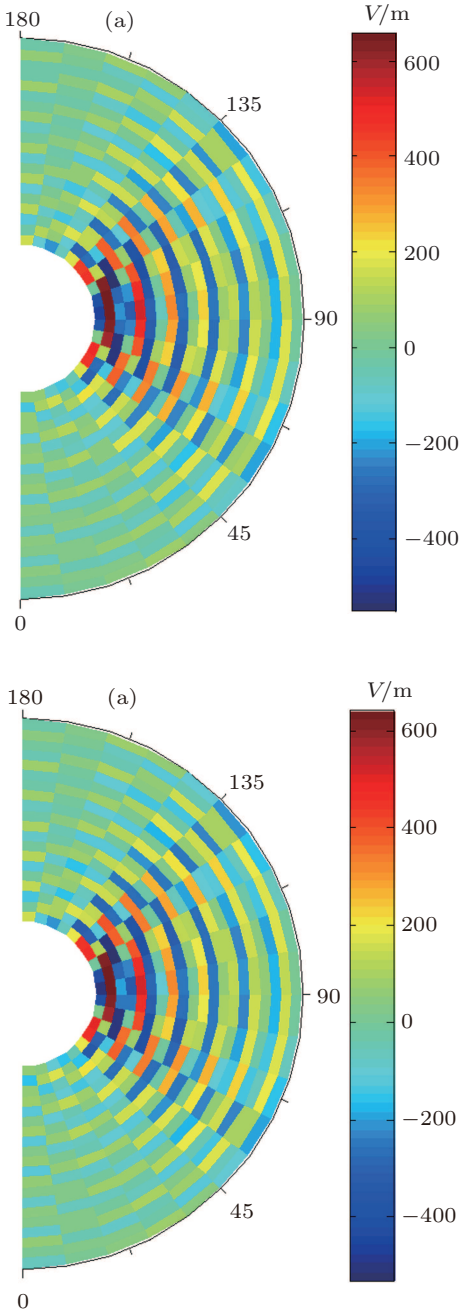


Fig. 10. (color online) E_θ fields for the dipole near a conducting sphere in V/m. (a) Analytical result. (b) Numerical result.

6. Conclusion

In this paper, we proposed an HO-FDTD scheme in the spherical coordinates. The stability and numerical dispersion property of the algorithm are analyzed. Compared with the FDTD method, the proposed method has a low sampling rate which can significantly reduce the numerical phase error, and compared with the MRTD method, the HO-FDTD method can also gain a general advantage. Furthermore, the Berenger's PML absorbing boundary condition is developed for the spherical HO-FDTD scheme. Three validating examples show that the PML can provide a satisfactory absorbing performance.

References

[1] Manry C W, Broschat S L and Schneider J B 1995 *Appl. Comput. Electromagn. Soc. J.* **10** 17

[2] Young J L 1996 *IEEE Trans. Anten. Propag.* **44** 1283

[3] Roberts A R and Joubert J 1997 *Electron. Lett.* **33** 32

[4] Hadi M F and Piket-May M 1997 *IEEE Trans. Anten. Propag.* **45** 254

[5] Lan K, Liu Y and Lin W 1999 *IEEE Trans. Electromag. Compatibility* **41** 160

[6] Zhang J and Chen Z 2000 *IEEE Anten. Propag. Soc. Int. Symp.*, Salt Lake City, USA, p. 1510

[7] Hirono T, Lui W, Seki S and Yoshikuni Y 2001 *IEEE Trans. Microw. Theory Tech.* **49** 1640

[8] Shao Z H, Shen Z X, He Q Y and Wei G W 2003 *IEEE Trans. Microw. Theory Tech.* **51** 856

[9] Kantartzis N V and Tsiboukis T D 2004 *IEEE Trans. Electromag. Compatibility* **46** 2

[10] Shlager K L and Schneider J B 2004 *IEEE Trans. Anten. Propag.* **52** 1095

[11] Chun S T and Choe J Y 2005 *IEEE Trans. Anten. Propag.* **53** 2237

[12] Wang S, Shao Z and Wen G 2007 *IEEE Microwave Wireless Compon. Lett.* **17** 316

[13] Chen Y W, Liu Y W, Chen B and Zhang P 2013 *IEEE Trans. Anten. Propag.* **61** 4695

[14] Taflove A *Computational Electrodynamics*: *The Finite-Difference Time-Domain Method* (Boston: Artech House)

[15] Cheong Y W, Lee Y M, Ra K H, Kang J G and Shin C C 1999 *IEEE Microwave Guid Wave Lett.* **9** 297

[16] Fujii M and Hoefer W J R 2000 *IEEE Microwave Guid Wave Lett.* **10** 125

[17] Daubechies I 1992 *Ten Lectures on Wavelets* (Philadelphia, PA: SIAM)

[18] Holland R 1983 *IEEE Trans. Nucl. Sci.* **30** 4592

[19] Krumpholz M and Katehi Linda P B 1996 *IEEE MTT* **44** 555

[20] Teixeira F L and Chew W C 1997 *IEEE Microwave Guide Wave Lett.* **7** 285

[21] Potter M E, Okoniewski M and Stuchly M A 2002 *IEEE Microwave Wireless Compon. Lett.* **12** 142